arXiv:astro-ph/0601620v2 28 Mar 2006

XMM–Newton View of the $z > 0$ Warm–Hot Intergalactic Medium Toward Markarian 421

Rik J. Williams[1], Smita Mathur[1], Fabrizio Nicastro[2,3,4], Martin Elvis[2]

williams,smita@astronomy.ohio-state.edu

ABSTRACT

The recent detection with *Chandra* of two warm–hot intergalactic medium (WHIM) filaments toward Mrk 421 by Nicastro et al. provides a measurement of the bulk of the "missing baryons" in the nearby universe. Since Mrk 421 is a bright X-ray source, it is also frequently observed by the *XMM–Newton* Reflection Grating Spectrometer (RGS) for calibration purposes. Using all available archived *XMM* observations of this source with small pointing offsets ($< 15''$), we construct the highest–quality *XMM* grating spectrum of Mrk 421 to date with a net exposure time (excluding periods of high background flux) of 437 ks and ~ 15000 counts per resolution element at 21.6 Å, more than twice that of the *Chandra* spectrum. Despite the long exposure time neither of the two intervening absorption systems is seen, though the upper limits derived are consistent with the *Chandra* equivalent width measurements. This appears to result from (1) the larger number of narrow instrumental features caused by bad detector columns, (2) the degraded resolution of XMM/RGS as compared to the *Chandra*/LETG, and (3) fixed pattern noise at $\lambda \gtrsim 29$ Å. The non–detection of the WHIM absorbers by XMM is thus fully consistent with the *Chandra* measurement.

Subject headings: intergalactic medium — X-rays: general — cosmology: observations

[1]Department of Astronomy, The Ohio State University, 140 West 18th Avenue, Columbus OH 43210, USA

[2]Harvard–Smithsonian Center for Astrophysics, Cambridge, MA, 01238, USA

[3]Instituto de Astronomía, Universidad Autónomica de México, Apartado Postal 70-264, Ciudad Universitaria, México, D.F., CP 04510, México

[4]Osservatorio Astronomico di Roma, Istituto Nazionale di Astrofisica, Italy

1. Introduction

Most of the baryons that comprise 4% of the mass–energy budget of the universe are found in the intergalactic medium (IGM), primarily appearing as the Lyman–alpha "forest" in high–redshift quasar spectra (Weinberg 1997). At more recent times ($z \lesssim 2$) the process of structure formation has shock–heated the IGM to temperatures of $\sim 10^{5-7}$ K, thus rendering the hydrogen nearly fully ionized and producing (at most) broad, extremely weak Lyman–alpha absorption (e.g. Sembach et al. 2004; Richter et al. 2004). Known as the warm–hot intergalactic medium (WHIM), this phase is predicted to contain roughly half of the baryonic matter at low redshifts (Cen & Ostriker 1999; Davé et al. 2001). Its extremely low density (typically $\delta \sim 10 - 100$) precludes the detection of WHIM thermal or line emission with current facilities, so the only way to directly measure these "missing" baryons is through far–ultraviolet and X-ray spectroscopic measurements of absorption lines from highly ionized heavy elements (Perna & Loeb 1998; Hellsten et al. 1998; Fang, Bryan, & Canizares 2002).

Several early attempts to detect these intervening WHIM absorbers in X-rays (e.g. Fang et al. 2002; Mathur, Weinberg, & Chen 2003; McKernan et al. 2003) and more recent surveys (Fang et al. 2005) yielded only tentative detections at best. Intervening Lyman–alpha (Shull et al. 1996; Sembach et al. 2004) and O VI (e.g. Savage et al. 2002) absorbers had also been seen in *FUSE* and HST quasar spectra, but their ionization states and possible galactic halo origins (e.g. Tumlinson et al. 2005) are quite uncertain. These uncertainties are largely mitigated with the recent detection by Nicastro et al. (2005a,b) of two X-ray absorption systems at $z = 0.011$ and $z = 0.027$ along the line of sight to the blazar Mrk 421. These filaments account for a critical density fraction of $\Omega_{\rm WHIM} = 0.032^{+0.042}_{-0.021}$, fully consistent with the mass of the missing baryons in the local universe (albeit with large uncertainties). While future proposed missions such as *Constellation–X*, *XEUS*, or *Pharos* (Nicastro et al., in preparation) will be able to measure $\Omega_{\rm WHIM}$ to far greater precision with detections of numerous weaker X-ray forest lines, the Nicastro et al. (2005a, hereafter N05) results present a key early confirmation of numerical predictions using observational capabilities that are *currently* within our grasp — hence any test of their correctness is of great importance.

Although each of these two absorption systems was detected with high confidence through multiple redshifted X-ray absorption lines, the *individual* absorption lines were generally quite weakly detected, mostly at the $2 - 4\sigma$ level. Moreover, while they employed high–quality *Chandra* and *FUSE* data taken during exceptionally bright outbursts of Mrk 421, the many archived *XMM–Newton* observations of this source were not included in the analysis. With roughly twice the effective area of *Chandra*/LETG, *XMM*/RGS is in principle superior for X-ray grating spectroscopy between $\sim 10 - 40$ Å; however, its slightly worse resolution (approximately 60 mÅ FWHM, versus 50 mÅ for *Chandra*/LETG), higher sus-

ceptibility to background flares, and multitude of narrow instrumental features can present serious complications for WHIM searches.

Independent confirmation of the *Chandra* results with a separate instrument like *XMM* is thus important. While some groups have searched for WHIM features in a limited number of *XMM* Mrk 421 spectra (e.g., Ravasio et al. 2005), a complete and systematic analysis has yet to be performed. Here we present a search for $z > 0$ WHIM features employing all "good" observations of Mrk 421 available in the *XMM* archive, and a comparison of these results to those presented by N05.

2. Data Reduction and Measurements

We searched the *XMM* archive for all Mrk 421 Reflection Grating Spectrometer (RGS) data. Although 31 separate observations were available, 16 had pointing offsets $\Delta\theta \gtrsim 60''$ while the rest were offset by less than $15''$. Since spectral resolution and calibration quality can degrade at large offsets, we only included those with $\Delta\theta < 15''$. One extremely short observation (0158971101, with $t_{\rm exp} = 237\,{\rm s}$) was also excluded to simplify the data reduction process. Using the standard *XMM* Science Analysis System version 6.5.0 routines[1], RGS1 light curves were built for the remaining 14 "good" observations (see Table 1), and the spectra were reprocessed to exclude periods of high background levels and coadded. These combined, filtered RGS1 and RGS2 spectra have effective exposure times of $\sim 440\,{\rm ks}$ and over 9×10^6 combined RGS1+RGS2 first–order counts between $10 - 36\,{\rm \AA}$ with ~ 15000 counts per $0.06\,{\rm \AA}$ resolution element in RGS1 near $21\,{\rm \AA}$, over twice that in the N05 Mrk 421 *Chandra* spectrum.

We first used the spectral fitting program *Sherpa*[2] to fit a simple power law plus Galactic foreground absorption model to the RGS1 and RGS2 data; however, at such high spectral quality the RGS response model does not appear to be well–determined, and large residuals remained. For line measurements, we thus only considered $\sim 2\,{\rm \AA}$ windows around each wavelength of interest, using a power law to independently model the RGS1 and RGS2 continua within each window and excluding the strongest narrow detector features (with typical widths of $70\,{\rm m\AA}$ or less). None of the intervening absorption lines were apparent through a visual inspection of the *XMM* spectrum, though several of the $z = 0$ lines reported by Williams et al. (2005) could be seen clearly.

[1]See http://xmm.vilspa.esa.es/sas

[2]http://cxc.harvard.edu/sherpa/

A narrow Gaussian absorption line (FWHM= 5 mÅ) was included in the model for each line measurement or upper limit reported by N05. When convolved with the RGS instrumental response these absorption lines appeared broadened to the RGS line spread function (LSF) widths (typically FWHM= 60−70 mÅ; den Herder et al. 2001). The 2σ upper limits on all equivalent widths were then calculated (allowing the central line wavelengths to vary within the 1σ errors reported by N05). Since the shapes of the RGS1 and RGS2 instrumental responses are quite different, these limits were calculated using both a joint fit to the RGS1+RGS2 spectra as well as the individual RGS1 and RGS2 spectra. It should be noted that wherever one RGS unit is unusable, the total response is effectively halved, at which point it has a similar effective area to *Chandra*/LETG. The resulting equivalent width limits are listed in Table 2.

3. Discussion

Figure 1 shows the spectral windows used to determine upper limits on the N05 measured lines, with the data (black), continuum fit (blue), *Chandra* measurements and limits (N05; red solid and dotted lines respectively), and *XMM* limits (green) overplotted. In all cases, the N05 measurements (or 3σ upper limits) appear to be consistent with the 2σ upper limits we have derived directly from the *XMM* data, as shown in the figure and listed in Table 2. The O VII line at $z = 0.027$ looks as though it might be visible in the spectrum, but this is most likely due to the weak instrumental feature at ~ 22.1 Å. For two lines (N VII and N VI at $z = 0.027$) the *XMM* 2σ upper limits are approximately equal to the N05 best–fit measurements, but since the N05 values are quite uncertain this result is still consistent.

Why, then, with $2 - 4$ times the counts per resolution element, was *XMM* unable to detect the intervening absorption systems seen by *Chandra*? Several factors appear to have been involved in this non–detection, primarily: (1) narrow instrumental features caused by bad detector columns, (2) the broader LSF as compared to *Chandra*/LETG, and (3) fixed–pattern noise at long wavelengths:

1. While broad instrumental features can be taken into account by modifications to the continuum model (as in N05), it is difficult or impossible to distinguish narrow features from true absorption lines; thus, any line falling near one of the detector features shown in Figure 2 can easily be lost[3]. This was responsible for the non-detection of the $z = 0.011$ O VII Kα line. Although it was the strongest line reported by N05,

[3]These response file data can be found at http://www.astronomy.ohio-state.edu/∼smita/xmmrsp/

its wavelength falls directly on a narrow RGS1 feature and within the non–functional CCD4 region on RGS2, thereby preventing this line from being detectable with either RGS. Since 18% of the wavelength space for studying redshifted O VII ($\lambda > 21.6\,$Å) toward Mrk 421 is directly blocked by these narrow features (with this number climbing to about 60% if resolution elements immediately adjacent to bad columns are included), these bad columns present the single greatest hindrance to *XMM*/RGS studies of the WHIM.

2. Even for lines where both RGS1 and RGS2 data are available and the instrumental response appears to be relatively smooth, the lower resolution of *XMM* contributes to the nondetectability of the weaker $z > 0$ absorption lines. Figure 3 shows the LSFs for both *XMM*/RGS1 (solid) and *Chandra*/LETG assuming an unresolved line with $W_\lambda = 10\,$mÅ at 21.6 Å. While the core of the RGS1 response is $\sim 20\%$ broader than that of the LETG, the RGS1 LSF has extremely broad wings: only 68% of the line flux is contained within the central 0.1Å of the RGS1 LSF, as opposed to 96% for the LETG. This reduces the apparent depth of absorption lines by about a factor of two as compared to *Chandra*/LETG, severely decreasing the line detectability.

3. At long wavelengths ($\lambda \gtrsim 29\,$Å) strong fixed–pattern noise is apparent as a sawtooth pattern in the instrumental response, strongly impeding the detection of species such as N VI and C VI. Indeed, in these wavelength regimes (the lower two panels of Figure 1), the N VI and C VI absorption lines are nearly indistinguishable from the continuum.

4. Conclusion

We have presented the highest signal–to–noise coadded *XMM* grating spectrum of Mrk 421 to date, incorporating all available archival data. This spectrum serves as an independent check on the recent detection of two $z > 0$ WHIM filaments by N05. While none of the *Chandra*–detected absorption lines are seen in the *XMM* spectrum, the upper limits derived from the *XMM* data are consistent with the equivalent widths reported by N05 (even though the *XMM* data contain a larger number of counts), and hence do not jeopardize the validity of the *Chandra* measurement. The non–detections can be attributed primarily to narrow instrumental features in RGS1 and RGS2, as well as the inferior spectral resolution of *XMM* and fixed–pattern noise at longer wavelengths. This underscores the extreme difficulty of detecting the WHIM, illustrates how the aforementioned (apparently small) effects can greatly affect the delicate measurement of weak absorption lines, and re–emphasizes the importance of high resolution and a smooth instrumental response function for current and future WHIM absorption line studies.

We thank the *XMM* team for their efforts on this excellent mission, the helpdesk staff for their assistance with the data reduction, and the anonymous referee for helpful comments. This research is based on archival data obtained with XMM-Newton, an ESA science mission with instruments and contributions directly funded by ESA Member States and NASA. RJW is supported by an Ohio State University Presidential Fellowship, and FN acknowledges the support of NASA Long–Term Space Astrophysics Grant NNG04GD49G.

REFERENCES

Cen, R., & Ostriker, J. P. 1999, ApJ, 514, 1

Davé, R., et al. 2001, ApJ, 552, 473

den Herder, J. W., et al. 2001, A&A, 365, L7

Fang, T., Marshall, H. L., Lee, J. C., Davis, D. S., & Canizares, C. R. 2002, ApJ, 572, L127

Fang, T., Bryan, G. L., & Canizares, C. R. 2002, ApJ, 539, 532

Fang, T., Canizares, C. R., & Marshall, H. L. 2005, ApJ, 633, 61

Hellsten, U., Gnedin, N. Y., & Miralda–Escudé, J. 1998, ApJ, 509, 56

Mathur, S., Weinberg, D. H., & Chen, X. 2003, ApJ, 582, 82

McKernan, B., Yaqoob, T., Mushotzsky, R., George, I. M., & Turner, T. J. 2003, ApJ, 589, L83

Nicastro, F., et al. 2005, ApJ, 629, 700

Nicastro, F., et al. 2005, Nature, 433, 495

Perna, R., & Loeb, A. 1998, ApJ, 503, L135

Ravasio, M., Tagliaferri, G., Pollock, A. M. T., Ghisellini, G., & Tavecchio, F. 2005, A&A, 438, 481

Richter, P., Savage, B. D., Tripp, T. M., & Sembach, K. R. 2004, ApJS, 153, 165

Savage, B. D., Sembach, K. R., Tripp, T. M., & Richter, P. 2002, ApJ, 564, 631

Sembach, K. R., Tripp, T. M., Savage, B. D., & Richter, P. 2004, ApJS, 155, 351

Shull, J. M., Stocke, J. T., & Penton, S. 1996, AJ, 111, 72

Tumlinson, J., Shull, J. M., Giroux, M. L., & Stocke, J. T. 2005, ApJ, 620, 95

Weinberg, D. H. 1997, ApJ, 490, 564

Williams, R. J., et al. 2005, ApJ, 631, 856

This preprint was prepared with the AAS LaTeX macros v5.2.

Table 1. *XMM–Newton* observation log

ID	Date	$t_{\rm exp}$[a] ks	$t_{\rm filt}$[b] ks	Rate[c] s^{-1}
0099280101	2000 May 25	63.8	21.2	15.7
0099280201	2000 Nov 01	40.1	34.1	5.4
0099280301	2000 Nov 13	49.8	46.6	15.3
0099280501	2000 Nov 13	21.2	17.8	17.2
0136540101	2001 May 08	38.8	36.1	11.7
0136540301	2002 Nov 04	23.9	20.5	11.7
0136540401	2002 Nov 04	23.9	20.1	13.6
0136540701	2002 Nov 14	71.5	62.8	16.4
0136541001	2002 Dec 01	70.0	58.1	8.3
0158970101	2003 Jun 01	43.0	25.3	9.0
0158970201	2003 Jun 02	9.0	6.6	9.7
0158970701	2003 Jun 07	48.9	29.9	5.4
0158971201	2004 May 06	65.7	40.5	19.5
0162960101	2003 Dec 10	30.0	17.5	9.8
TOTAL		572.3	437.1	12.2

[a]Total observation duration.

[b]Effective RGS1 exposure time after filtering for periods of high background levels.

[c]Average count rate in the filtered RGS1 first–order source spectral extraction region.

Table 2. Absorption line equivalent width measurements

Line	λ[a] Å	z[a]	$W_{\lambda,\mathrm{N05a}}$[a] mÅ	$W_{\lambda,\mathrm{R1}}$[b] mÅ	$W_{\lambda,\mathrm{R2}}$[b] mÅ	$W_{\lambda,\mathrm{R1+R2}}$[b] mÅ	Note
Ne IX$_{K\alpha}$	13.80 ± 0.02	0.026 ± 0.001	< 1.5	< 5.2	< 1.9	< 2.9	1
O VII$_{K\beta}$	19.11 ± 0.02	0.026 ± 0.001	< 1.8	< 2.5	< 2.1	< 1.5	
O VIII$_{K\alpha}$	19.18 ± 0.02	0.011 ± 0.001	< 4.1	< 7.6	< 5.8	< 4.1	
O VIII$_{K\alpha}$	19.48 ± 0.02	0.027 ± 0.001	< 1.8	$\cdots$	< 3.9	$\cdots$	2
O VII$_{K\alpha}$	21.85 ± 0.02	0.011 ± 0.001	$3.0^{+0.9}_{-0.8}$	$\cdots$	$\cdots$	$\cdots$	2,3
O VII$_{K\alpha}$	22.20 ± 0.02	0.028 ± 0.011	2.2 ± 0.8	< 3.9	$\cdots$	$\cdots$	3
N VII$_{K\alpha}$	25.04 ± 0.02	0.010 ± 0.001	1.8 ± 0.9	< 3.0	< 6.0	< 4.4	
N VII$_{K\alpha}$	25.44 ± 0.02	0.027 ± 0.001	3.4 ± 1.1	< 4.3	< 4.2	< 3.5	
N VI$_{K\alpha}$	29.54 ± 0.02	0.026 ± 0.001	3.6 ± 1.2	< 3.8	< 8.7	< 3.4	
C VI$_{K\alpha}$	34.69 ± 0.02	0.028 ± 0.001	2.4 ± 1.3	< 5.5	< 5.2	< 4.2	

[a] Line wavelength, redshift, and equivalent width measurements (or 3σ upper limits) from Nicastro et al. (2005a).

[b] 2σ equivalent width upper limits measured from the RGS1 only (R1), RGS2 only (R2), and joint (R1+R2) fits to the XMM–Newton spectrum, when available.

Note. — (1) A nearby chip gap in RGS1 renders this measurement unreliable, so only the RGS2 measurement was used in Figure 1; (2) Line was unmeasurable in RGS1 because of a detector feature; (3) Line was unmeasurable in RGS2 because of a detector feature.

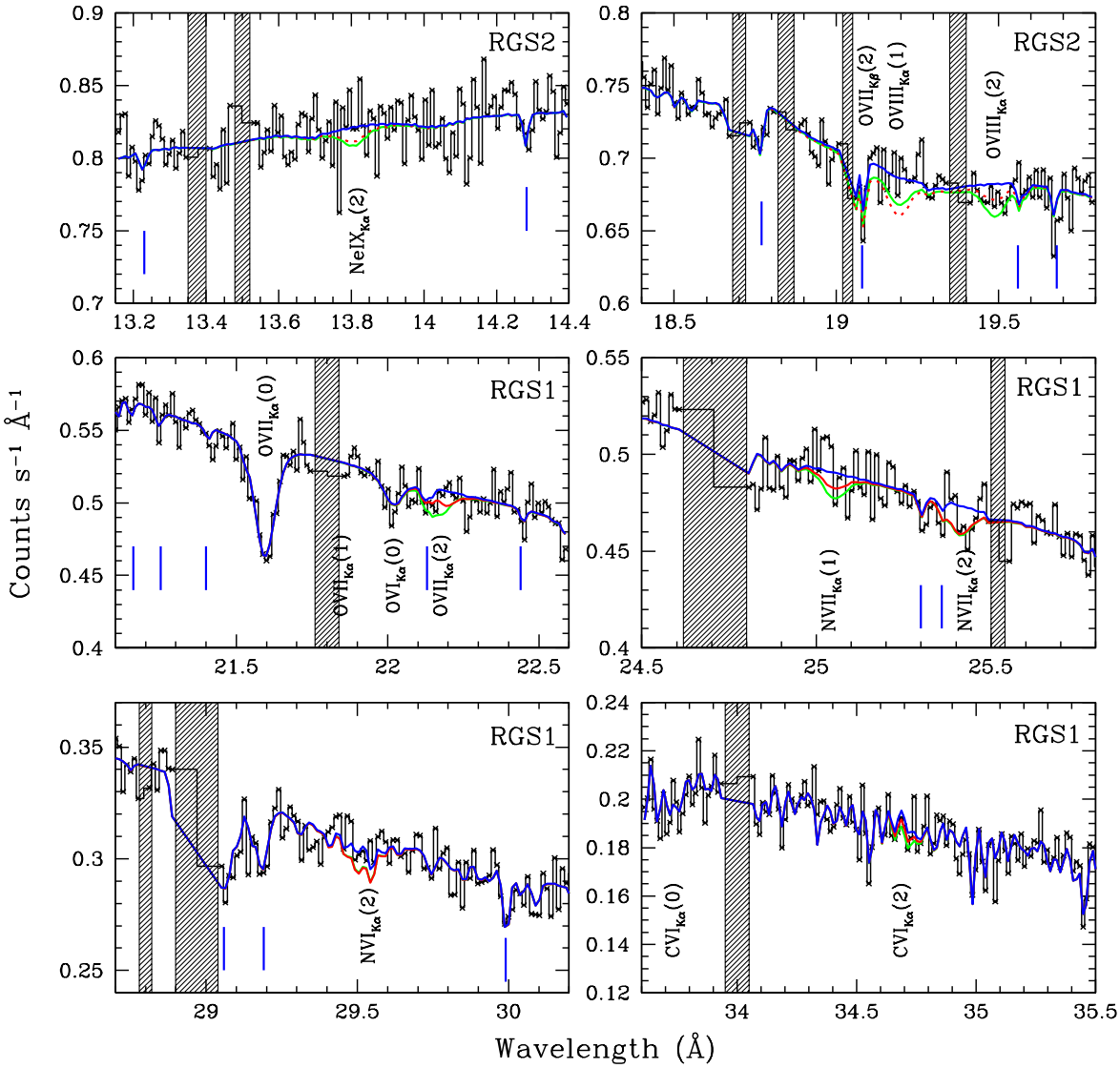

Fig. 1.— Portions of the XMM–Newton RGS spectrum of Mrk 421 (black histogram). The continuum fit is shown by the solid blue line, the green line depicts the 2σ upper limit on each measured species from XMM, and the red lines show the results of N05a (where their 3σ upper limits are shown as dashed lines, while solid lines indicate best–fit measurements). All N05a absorption line positions are labeled, with (1) and (2) denoting $z = 0.011$, and $z = 0.027$ lines respectively. Significant $z = 0$ lines are included in the continuum fit for consistency and labeled with (0), but not discussed further here. Regions that were excluded from the fit due to chip gaps and detector features are shaded; weaker instrumental features are marked with vertical blue ticks. Although joint fits using RGS1 and RGS2 were performed whenever possible, for display purposes only one or the other (indicated in the upper right–hand corner of each plot) is shown for each spectral region.

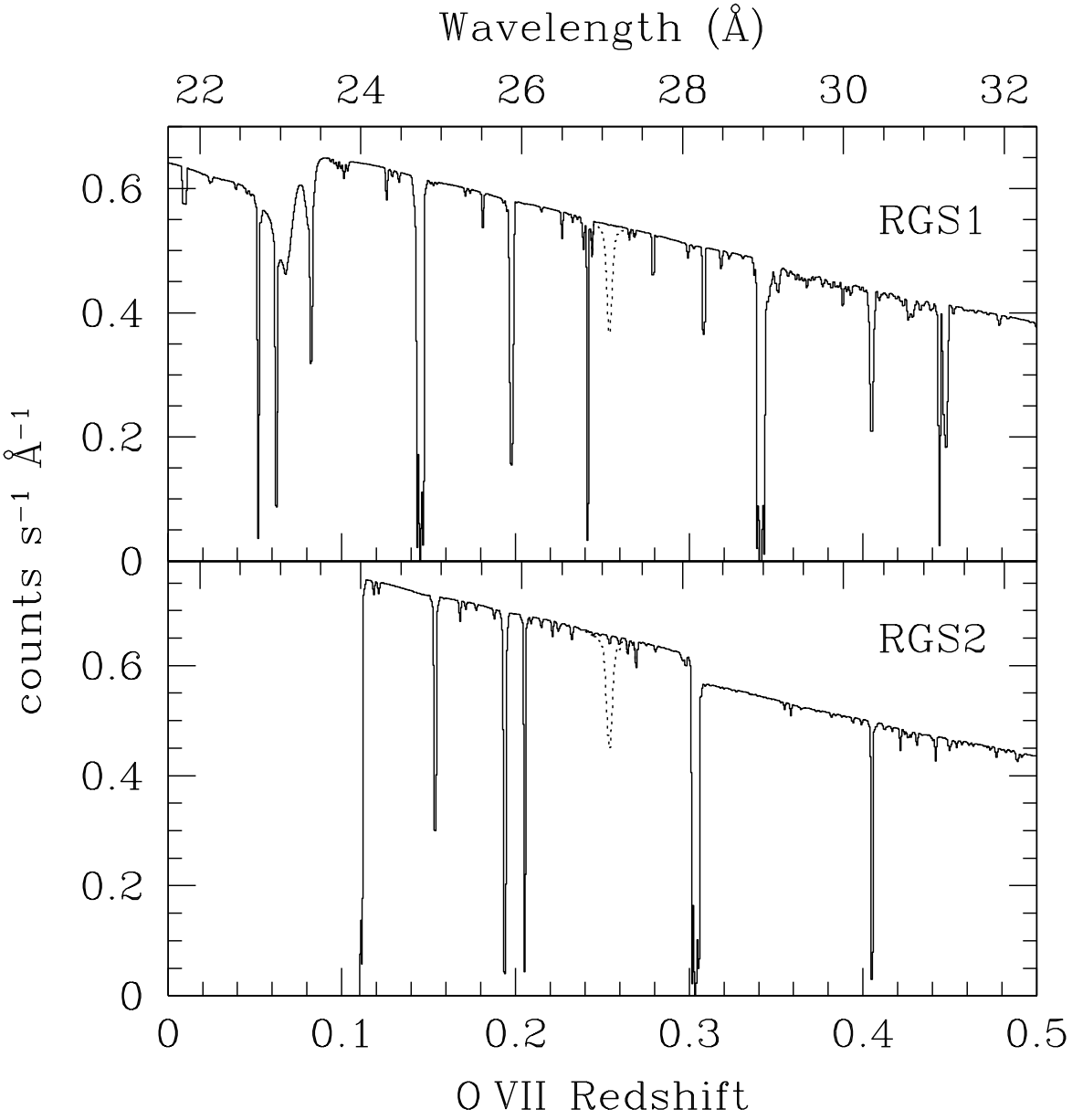

Fig. 2.— RGS1 (top panel) and RGS2 (bottom panel) instrumental response models for the O VII $z = 0 - 0.5$ region, as a function of wavelength (upper axes) and redshift relative to $\lambda = 21.602$Å (lower axes); a strong $z = 0.25$ line with $N_{\rm OVII} = 10^{16}\,{\rm cm}^{-2}$ ($W_\lambda = 36\,{\rm m\AA}$) is shown for reference.

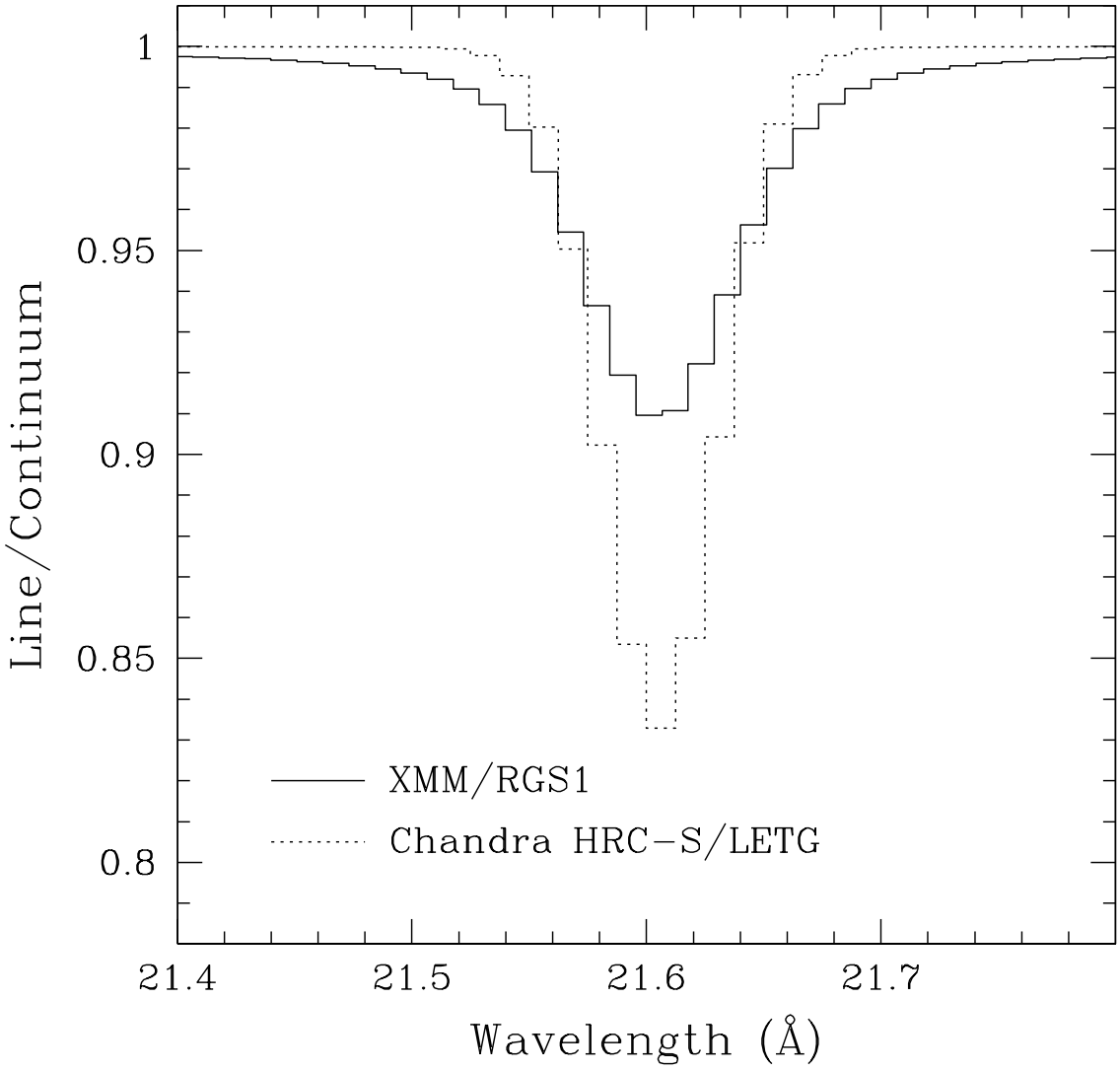

Fig. 3.— Comparison of the *XMM* RGS1 (solid) and *Chandra* HRC-S/LETG (dotted) line spread functions for a $W_\lambda = 10\,\mathrm{m\AA}$ unresolved absorption line at 21.602 Å.